RELATIONSHIP BETWEEN MICRO-STRUCTURE AND MECHANICAL PROPERTIES OF DISSIMILAR ALUMINUM ALLOY PLATES BY FRICTION STIR WELDING

by

Furkan SARSILMAZ *

Department of Mechatronics Engineering, Firat University, Elazıg, Turkey

Original scientific paper
https://doi.org/10.2298/TSCI170825271S

Friction stir welding can be applied to weld dissimilar aluminum alloys which have different chemical and mechanical properties without causing any weld defects under a wide range of welding conditions. In this study, AA2024-T3 and AA6063-T6 aluminum alloys were selected and successfully welded in butt position together using by friction stir welding. The welding trials were conducted using different rotational speed and traverse speed conditions also investigating their effect on mechanical and micro-structural behavior of friction stir welding joints. The micro-structural evolution of the material was analyzed by optical observations and scanning electron microscopy inspections of the weld cross-sections. Tension and fatigue studies were also employed to the study. On the other hand, the fracture characterizations of samples were examined by scanning electron microscopy. Fatigue tests were performed by using a resonant electro-mechanical fatigue testing machine by axial bending fatigue test procedure. The fatigue strength has been analyzed drawing S-N curves. Experimental results indicate that micro-structural and mechanical properties are significantly affected by changing welding parameters within the chosen range of welding conditions.

Key words: friction stir welding, aluminum alloys, mechanical properties

Introduction

Aluminum alloys with good formability, high mechanical strength, good heat transfer, and weight saving have been considered for military, shipbuilding, aerospace, automotive and rail industries, *etc.* [1]. The weldability properties of aluminum alloys itself and to other materials with conventional fusion welding process such as gas tungsten, arc, metal inert gas welding and electron-beam welding opens up the possibility to product unexpected phase propagation due to annealing and a series of negative metallurgical change occurs at the welding interface. Therefore, extensive care and precautions like pre and post heat treatment or quick welding speeds are required [2, 3]. These problems have been minimized by solid state welding processes, such as friction stir welding (FSW). Recently, developments in the welding technology for aluminum alloys such as ultrasonic and diffusion bonding, electric discharge bonding, friction welding, and FSW have been progressing by new researches [2-5]. The FSW is a solid-state process, which means that the base materials to be welded do not melt during the joining process. Always the frictional heat reaches below the melting temperature of materials [5, 6]. The FSW is a promising welding process that can produce low distortion, high quality, lower re-

* Author's e-mail: fursar@gmail.com

sidual stresses, fewer weld defects, and low cost joints between aluminum alloys. In addition, FSW finds wide spread industrial use as a mass production process for the joining of aluminum alloys which is a relatively new technique developed by the Welding Institute for the joining of aluminum alloys [4-7]. In this process, the material was essentially extruded around the tool by the large pressure and high deformation. However, this process achieves solid-state joining by locally frictional heat and plastic flow by rotation of the welding tool with resulting local micro-structure changes in aluminum alloys [7].

Nowadays, many studies on the micro-structure and mechanical properties of dissimilar types of aluminum alloy conducted usually to the temperature distribution, material flow and the effect of process parameters such as the tool profile, rotational and traverse speed on the friction stir welded joints [8]. These all have shown that the differences in aluminum alloys exhibit different friction stir weld ability [9, 10]. When the results of all works conducted up till now are taken into consideration, it can be seen that FSW method is the most applicable process for welding dissimilar metal couples [11-13]. Therefore, the aim of the present work is to study the relations between the micro-structure and mechanical properties of the joints around the welding parameters in order to determine the optimum welding condition for high quality friction stir welded joints.

Material and experimental procedure materials and tools properties

Two kind of aluminum alloy standards AA 2024-T3 and AA 6063-T6 plates with dimensions 200 × 100 mm and thickness of 8 mm were used in the present work as test material. The nominal chemical compositions and mechanical properties of test materials are given in tab. 1.

Table1. Chemical composition [wt.%] and mechanical properties of alloys

	Fe	Si	Cu	Mn	Mg	Zn	Ti	Hardness [HV]	σ_y [MPa]
AA2024-T3	0.50	0.50	4.4	0.65	1.6	0.25	0.15	139	324
AA6063-T6	0.30	0.35	0.10	0.10	0.45-0.9	0.10	0.05	81	214

A conventional milling machine was used for this purpose. The schematic illustration of FSW process is given fig. 1. Non-consumable tools made of high carbon steel have been used to fabricate the joints. The stirrer tool was produced D5 steel with conical triangular pin profile which was quenched-tempered to 60 HRC as also shown in fig. 1. The tool tilt angle was kept at 2.5° with rotating in the clockwise direction. A constant plunged depth position of the pin

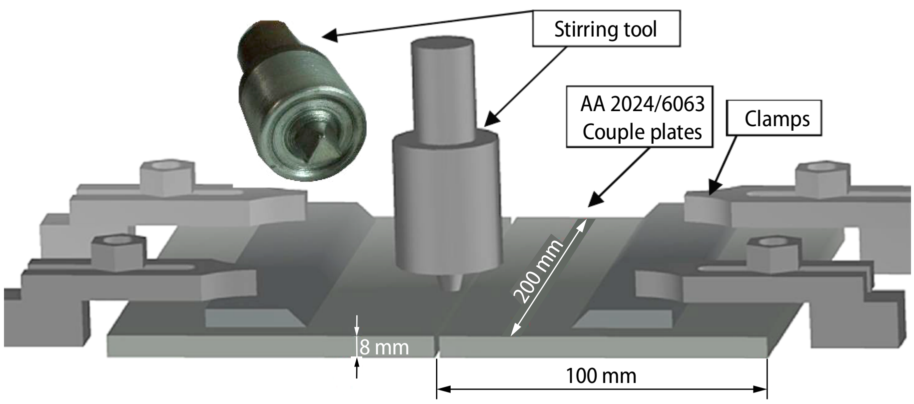

Figure 1. Schematic representation of the welding instrument and stirrer geometry

was used at all welding parameters during FSW [14]. Before welding, the kissing surfaces of plates were ground with grit paper to remove the oxide film and cleaned with acetone. During the FSW process, the welding parameters such as tool rotational speed and traverse speed were changed to explore their effects on welding quality as shown in tab. 2. The plate arrangement was selected that, the AA2024 alloy was on the advancing side of the tool while the AA6063 alloy was on the retreating one.

Table 2. The welding process parameters

Materials	Rotational speed [rpm]	Traverse speed [mm/min]	Sample number
AA2024/AA6063	900	125	S1
		160	S2
		200	S3
	1120	125	S4
		160	S5
		200	S6
	1400	125	S7
		160	S8
		200	S9

Micro-structure and fracture investigation

In order to determine micro-structural properties of these joints, the samples were cross-sectioned perpendicular to the weld interface using a water-cooling low speed saw. The cross-section of these joints was metallographically polished using diamond paste as final polish and then cleaned acetone. The specific etchant was used for optic micro-structural examination which solution consisting of 100 ml water, 2 ml nitric acid, 4 ml hydrofluoric acid, 4 ml hydrochloric acid, and applied for 180 second [15]. In addition, a SEM equipped with field emission gun (type JEOL-JSM 6500 F) has been employed to observe the samples surfaces morphology and also fractured surfaces which failure after by fatigue and tensile test samples.

Tensile tests examination

The tensile tests have been executed perpendicular to the weld direction having calibrated dimensions of 140 mm in length and 15 mm in width. For the standardization purpose, all samples were obtained by means of CNC machine. Figure 2 demonstrates the location of the test samples. For each weld condition, the tests were carried out at the room temperature using an Instron testing machine with crosshead speed of $1.67 \cdot 10^{-2}$ mm/s. The axial applied load was always perpendicular to the weld line. For drawing tensile test curves, executed three samples were employed to determine the average tensile test result for the same conditions.

Fatigue tests examination

A resonant type electro-mechanical fatigue testing machine which called Test-Tronic manufactured by Rumul with a capacity of 25-50 kN load was employed in a high frequency (up to 250 Hz wave loading control) in order to accelerate the testing time. The high cycle fatigue test results have been obtained by axial bending fatigue test procedure. All tests carried out on transverse flat tensile samples extracted from butt joints, and are expressed as stress

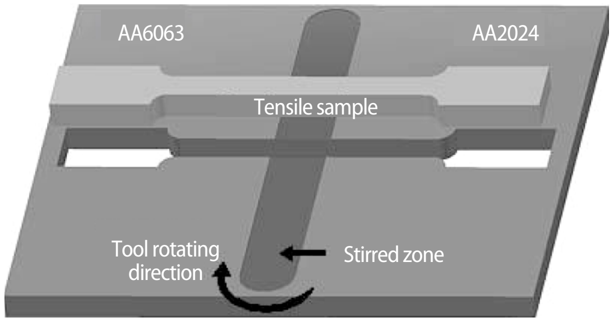

Figure 2. Illustration of tensile test sample location

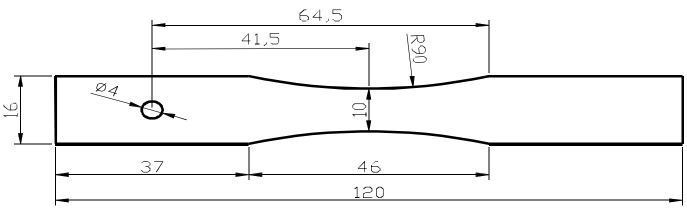

Figure 3. The fatigue test sample according to ASTM E466

amplitude Ds (MPa) *vs.* the corresponding life to failure (*i. e.* number of cycles). Nine friction stir butt-welded joints were used in the tests according to ASTM E-466 as shown in fig. 3. A sinusoidal load-time function was used, with the stress ratio. The cyclic tests were conducted under axial total stress control mode under fully in tension conditions R ($\sigma_{min}/\sigma_{max}$) fix to 0.1. The oscillation frequency was in the interval of 100-130 Hz in laboratory air. For each weld condition, at least seven test samples were employed. The evaluation of the fatigue properties of the welded couples was obtained by analyzing to fix fatigue strength data as S-N curve in diagram. In addition, a SEM equipped with field emission gun (type JEOL-JSM 6500 F) has been employed to observe the samples surfaces and the microscopic morphology and defects of the welded joints and the mechanics involved during fatigue failure have been analyzed.

Results and discussion

Micro-structure evaluation

A macroscopic overview of friction stir welded of AA 2024/AA6063 couple is given in fig. 4. It can be clearly seen that, very rough surface was formed for the 900 rpm sample in the friction stir welded zone. Void and defect-free welds were successfully obtained for the all samples. In addition, the top surface morphology of the friction stir welded zone formed fairly smoother with an increasing in the tool traverse speed. This result shows that there are optimum tool rotation/traverse speeds in order to obtain defect-free welds for the dissimilar FSW between 2024-T3 and 6063-O alloy plates.

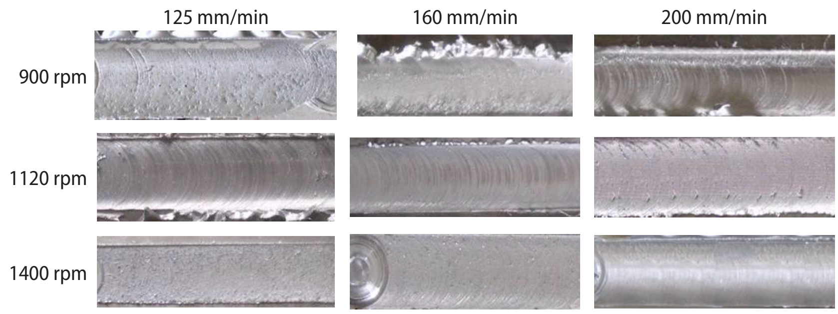

Figure 4. Top surface views of FSW sample at different welding conditions

The samples were cross-sectioned perpendicular to the joint line for metallurgical investigations. The metallographic observations tell us, the welding zone during FSW process is quite different than other solid-state welding techniques [16]. A detailed investigation of figs. 5 and 6 gives us a comparative optical micrograph of friction welded samples produced using triangular pin tool as S1 and S6, respectively. The S1 and S6 were chosen for sample representation to show the welded interface because of their evident micro-structural differences. It seems from the both photos, there are no micro cracks, micro voids and unbounded regions in the welded interface and a sound weld was found. A detailed investigation of fig. 5 tells us there are different morphologies of the micro-structure at interface zone of the weld processed joint. The weld region can be classified into four main different regions: parent metal (PM), thermo-mechanically affected zone (TMAZ), heat affected zone (HAZ), and the dynamically re-crystallized stir zone (SZ). These regions also reported by Jata and Semiatin [17]. The width of these regions was varied as a result of the relation between welding parameters such as rotational speed and traverse speed. The simultaneously effects of traverse and rotational speeds lead to a variation in temperature at the interface due to local heating resulting in narrower or wider HAZ.

All of the welds with producing using conical triangular pin revealed on the typical formation of the elliptical *onion* structure in the weld center depending on tool rotation speeds ranging from 900 to 1400 rpm. The SZ also included *onion rings* where the pin contacted the welded samples. The onion rings formation mechanism has been studied in the previous papers. According to Okamura *et al.* [18] the onion rings pattern was formed by the process of frictional heat due to rotation of the tool, in which forward movement extrudes metal around the retreating side of the tool. The onion rings feature was observed in SZ and corresponded to the selecting triangular pin tool parameter [19]. The amount of onion rings increasing as the traverse speed increasing. However, the onion ring blank increased with decreasing traverse speed. Both figs. 5 and 6 illustrate the enlarged micro-structures of the onion ring patterns with different welding condition. Onion ring patterns was characterized by the lamellar like structures stacked by the two materials.

In addition, the parameters which generated higher frictional heat such as low traverse speed (125 mm/min) and high rotational speed (1400 rpm) exhibited wider weld nugget than other parameters. As a consequence of that, the micro-structural transformation level of welding region increased proportionally. It is well known that heat input increases with increasing the rotational speed and decreasing travel speed during FSW. The higher temperature and severe forging deformation results in grains smaller than the base metal. The SZ had a fine equiaxed grain structure, see fig. 6. In all the FSW literature on aluminum alloys, the initial elongated grains of the parent materials are converted to a new equiaxed fine grain structure. This figure also shows the deformation directions included in grains in the TMAZ and the regions adjacent to the TMAZ is the HAZ. At higher magnifications the optical micrographs showed very fine equiaxed grains in the dynamically re-crystallized SZ, see fig. 6(a).

Moreover, fig. 5 also illustrates the micro-structure of TMAZ and SZ taken from at the interface zone of S1. The boundary between TMAZ and SZ clearly separates from one another in a line which resembles a vase. This vase geometry formation was attributed to extreme deformation and frictional heat occurred between weldment and the tool pin. Scialpi *et al.* [19] and Jata *et al.*[20] concluded that, the peak welding temperatures on the top surface are almost the same for all welding conditions. However, the peak temperature of generating the shoulder on the top surface is higher than the bottom surface which exposing minimum frictional area due to triangular pin surface. The formation of this vase geometry can be attributed that *these* extreme *temperature differences*.

Summarize the welding conditions, it is thought that since a larger frictional area must generate a larger amount of friction heat for these dissimilar types samples. The micro-structural transformation with frictional heat related to increasing rotational speed and low traverse speed, it was appeared high deformation level and as a result of this, the grains tended to forge with coarsing in all the samples.

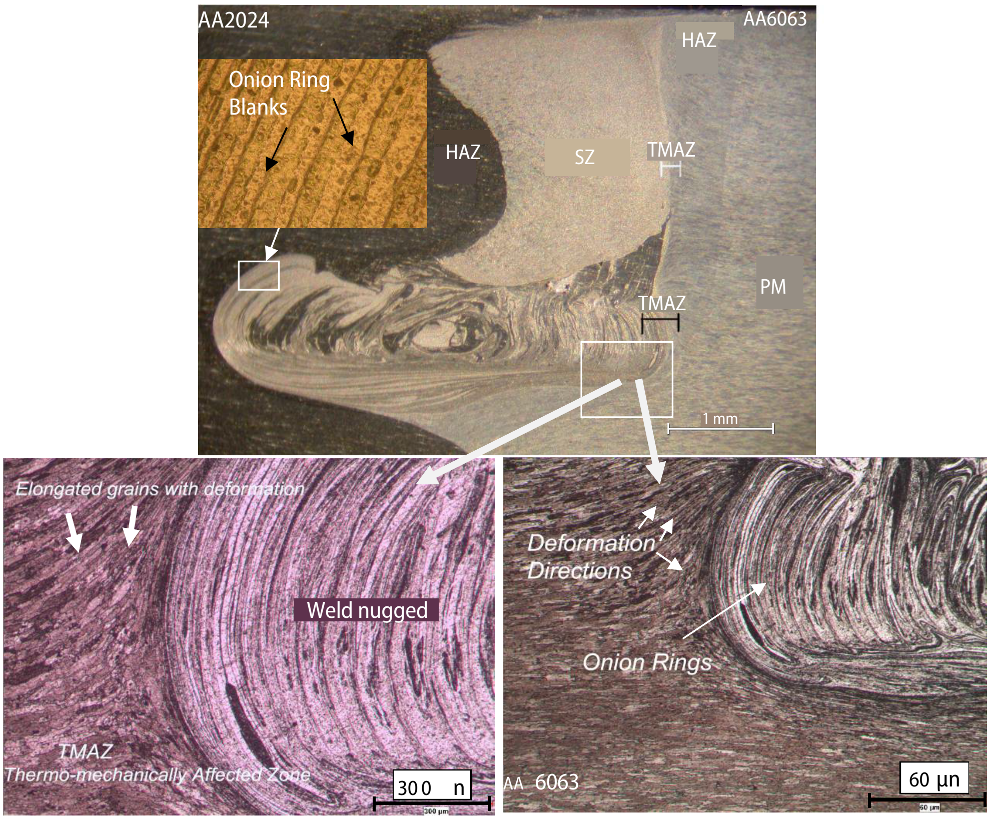

Figure 5. The macro illustration of regions and micro-structural formation of S1
(*for color image see journal web site*)

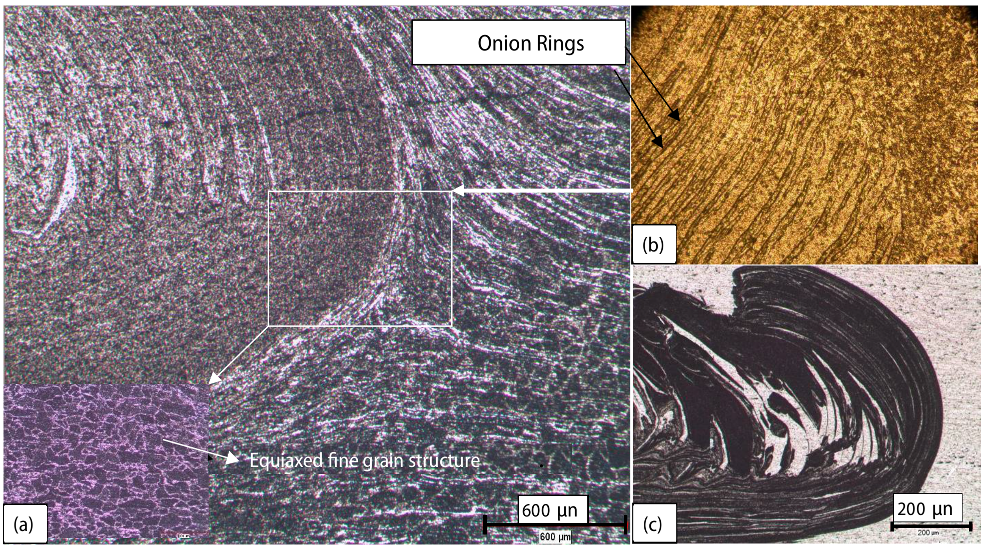

Figure 6. The micro-structural formation of S6 (a) the onion ring blanks (b), and macro illustration of weld nugget (c) (*for color image see journal web site*)

Tensile properties

At different welding conditions the tensile test response of couple results, transverse to the welding directions of the AA2024 and AA6063 joined by FSW is shown in fig. 7. The best groups of the welded samples are S3, S6, and S9 recorded. The highest tensile strength reaches for S3 sample as 348 MPa which was 74% of the tensile strength of the AA2024 base metal (470 MPa). However, an increasing in tensile strength is present approximately 45% greater than the base tensile strength of AA6063 (241 MPa). The elongation of the best sample was recorded as 13% which nearly below that of the base metals, *i. e.* in the range 14-21%. The mechanical tensile results of the best friction stir welded sample and parent couples are given in tab. 3.

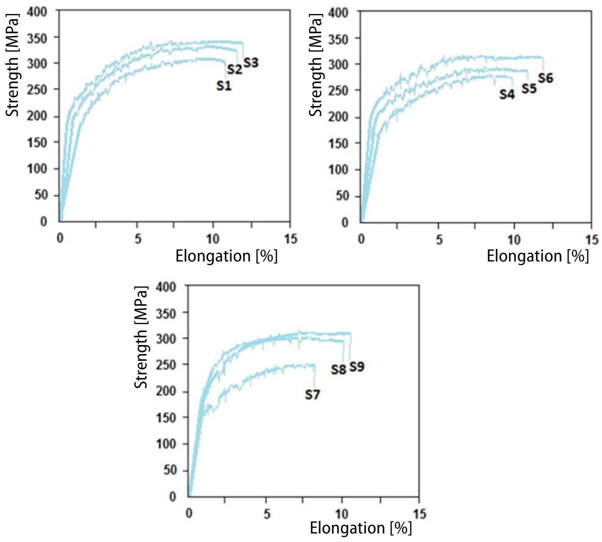

Figure 7. Tensile strength of friction stir welded samples at different welding conditions

Table 3. Mechanical properties of the 2024-6063 couples compared with those proper of the parent materials

Material	Yield strength [MPa]	Ultimate tensile strenght [MPa]	Elongation, ε [%]
AA 2024 T4	324	470	21
AA 6063 T6	214	241	14
2024- 6063 (best recorded at S3 sample)	238	348	13

This result indicated that the best welding parameter performed at 900 rpm and 200 mm/min traverse speed. Therefore, the highest levels of selected factors were found the optimal conditions. The tensile strength of the friction stir welded samples has shown a strong dependency on pin travel speed, as shown in fig. 7. Some of curves were changing into each other depend on higher or lower traverse speed when selected constant rotational speed. This is due to the heat input and heavy plastic deformation that occurred at the welding interface as a result of pin traverse speed. On the other hand, all the samples fractured beside the HAZ zones of the welds, always close to the 6063 side. This is in accordance with the classical mechanical behavior of these kinds of welded plates in which, from a micro-structural point of view, the mechanical response of the SZ results fairly higher than both TMAZ and HAZ because of the grain dimension differences and the precipitates intensity at the interfaces. As a consequence of this effect, all failures naturally occurred at HAZ location.

The tensile test results should be evaluated with the effects of both rotational and traverse speeds. The strength of samples slightly decreased with both higher rotational speed and lower traverse speed. Presenting literature reports that, a higher bonding temperature results in profuse inter-diffusion and better coalescence of mating surface [21]. However, increasing bonding temperature due to both higher rotational and lower traverse speed also promotes the growth of coarsing grains and precipitations at the interface. This case gives rise to the bond strength adversely. In this way the low values of elongation and tensile strength can be attributed to presence of coarsed grains at the HAZ location. It could be said that, the rotational and traverse speed had a strong impact on productivity of friction stir welded aluminum alloy

In the comprehending of the micro-structural effects on fracture properties some SEM observations were performed on the fractured surfaces of the tested samples. As shown fig. 8, the fracture surface of the AA2024/AA6063 joint of S3, S6, and S9 tested in tension perpendicular to welding direction was appeared with a broad population of microscopic voids of different dimensions and shapes. At room temperature material showed some ductility with fracture and revealed local ductile characterization. The fractographic analyses of the tensile tested surfaces revealed that the size distribution of ductile dimples became more circular and wider with higher rotational speed.

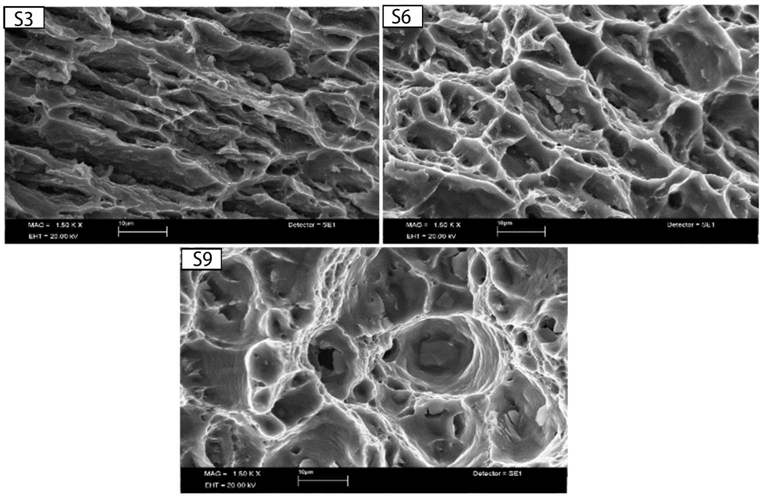

Figure 8. Tensile sample fracture surfaces of the different welded conditions showing voids shape and population

Fatigue properties

The fatigue resistance of both base material and welded joints in all conditions are shown as S/N curves in fig. 9. The fatigue graphics show a trend of decreasing cyclic stress amplitude with increasing fatigue life which represents general behavior for the aluminum alloys. A large number of fatigue tests have been done and the credibility under fatigue data are easily attested even considering the random character of the Wohler curves. The fatigue strength of joints with a FSW line inclined to the applied stress can be evaluated using data from joints with a FSW line perpendicular to the applied stress when the joints have no defects such as kissing bonds or welding cracks.

The fatigue tests were design to investigate the fatigue characteristics of dissimilar 2024/6063 alloys. All samples were loaded according to different welding parameters such as traverse and rotational speeds, corresponding to an R-ratio of 0.1. For the friction stir welded 6063-T6, it was found that for 68% and 70% of the yield stress the fatigue life is considered infinite considering some of literature [22]. In the present study, the applied stress levels were

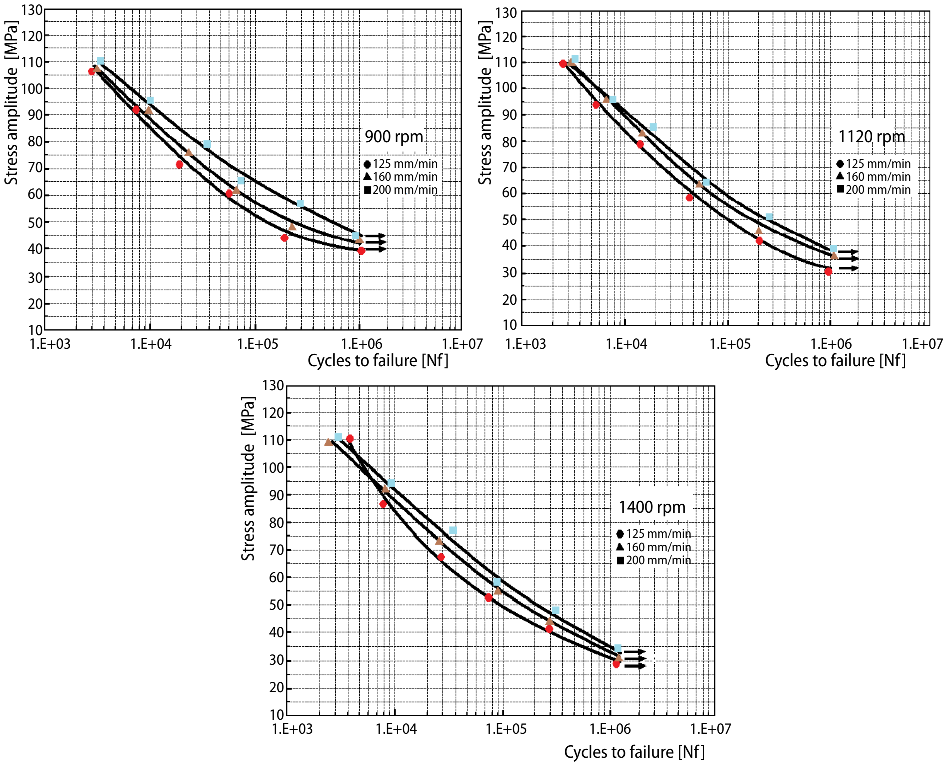

Figure 9. Endurance fatigue curves (S/N) of the 2024-6063 couples joined by FSW

designed to have fatigue lifetime of the samples between $1\cdot10^3$ and $1\cdot10^6$ cycles for database for stress-life approach *i. e.* the targeted lifetime of welded joints for the aimed aircraft application. The applied stress amplitudes were from 25 MPa to 110 MPa for the nine different types of welding conditions to get fatigue lifetime between $1\cdot10^3$ and $1\cdot10^6$. The number of cycles considered as a threshold for infinite life was 10^6 cycles.

The curves show a good fatigue behavior for 2024/6063 couples in lower rotational speed and higher traverse speed. For samples welded in different welding conditions, the number of cycles to failure increased with increasing stress amplitude. The best result was recorded at the sample welded 900 rpm and 200 mm/min as 45 MPa. While, the minimum fatigue strength as welded at 2024/6063 couple was about 29 MPa at 1400 rpm and 125 mm/min. In addition, the endurance of fatigue life both base metals are about 135/85 MPa, respectively, and very salient difference can be seen between results due to different welding conditions. It can also be seen that fatigue life of the FSW samples was always lower than that of the base material.

The fatigue lifes of samples which welded higher rotational speeds are slightly lower than that of other results. These results directly depend on the heat treatment properties of couples. Because it is clearly known that [11, 12, 18, 23] more frictional heat generated at higher rotational speed and lower traverse speed as previously mentioned. Thus strengthening precipitates dissolute as less strengthening properties and decrease the alloys mechanical properties during FSW. The lower fatigue life of the FSW material could be also related to the micro-structural modifications induced by the process, which consequently led also to a reduction in hardness and tensile strength properties. Micro-structural changes in the friction stir weld zone have been described in recently published papers [7-16]. With regard to age hardenable aluminum alloys, there have been some micro-structural studies [11, 14, 15, 21] of welds in alloys 2XXX, 6XXX, and 7XXX. These have demonstrated that the weld zone consists of fine, equiaxed grains and elongated, recovered grains. A HAZ was formed beside the weld zone. These reports [23-26] also explained the behavior of precipitates and dislocations associated with the temperature profile caused by frictional heat. The precipitates originally present in the base metal disappeared in the weld nugget and coarsened in the HAZ. This precipitate and dislocation behavior is considered to be the reason why a softened region is fractured near the weld zone during the all mechanical tests such as tensile and fatigue.

The failure samples from fatigue tests were also inspected for defects in the crack surface. In order to determining the fatigue crack initiation and propagation mechanisms, the crack surfaces of the samples were investigated using SEM. Over the $1 \cdot 10^6$ high cycle region, the initiation site of fatigue fracture was inner zone of the samples as shown in fig. 10. This behavior is observed for all the nine different condition of welds. The arrow in the fig. 10(c) indicates the initiation site of the fatigue fracture. It is clear that the initiation site is a near the surface of the samples. Moreover, the fracture surfaces of the samples tested above the 10^6 cycles are also shown in fig. 10(b) which indicate typical fatigue failure characteristics, with a single crack initiation site. Crack initiation is followed by fatigue crack propagation and finally overload

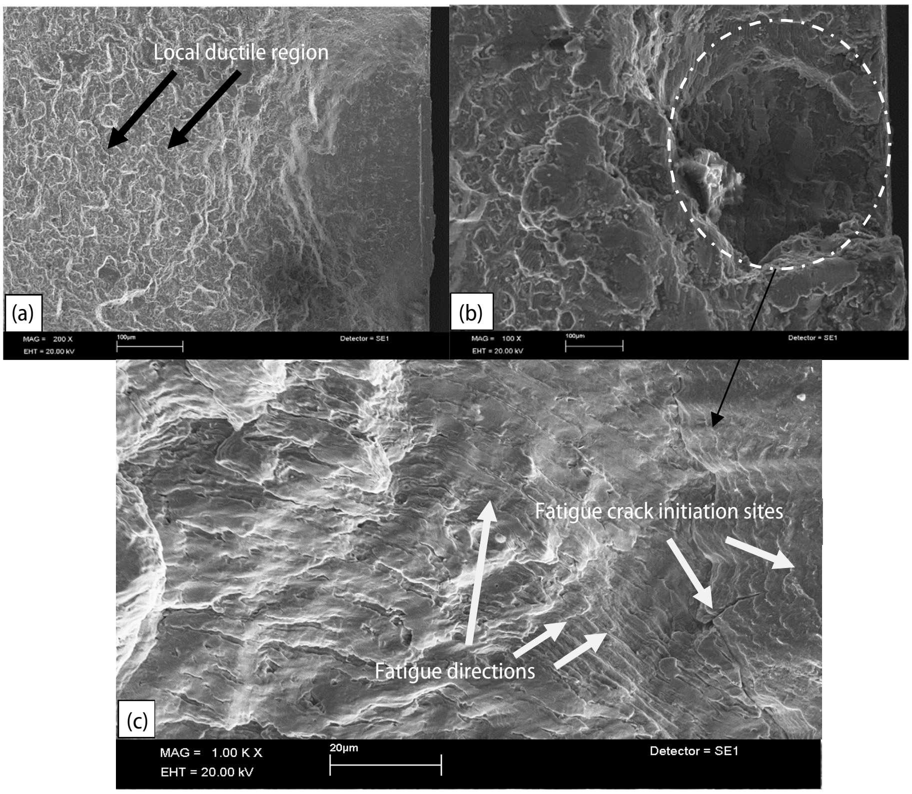

Figure 10. Fracture surface of relieved joints with local ductile region (a), the region of microscopic crack growth of relieved joints (b), and the arrows indicates crack initiation sites and fatigue directions (c)

failure. The fatigue cracks initiate at locations where grain boundaries have separated immediately adjacent to the sample surface [25-28]. At high cycle load, the microscopic crack growth has been associated with some degree of material ductile behavior (black arrows), showing the conventional fracture surfaces of very fine grain size structure into the welded section, see fig. 10(a). In addition, it can be clearly seen that from fig 10(b), in the high cycle loading range the fracture front is formed as a crater along the flow material lines produced by the tool during welding (as seen dotted circle region). Figure 10(c) also shows that, friction stir welded joints which exposed high cycle loads, included some of dispersed fatigue directions with fatigue crack initiation site at the broken surface

Conclusions

From the results of micro-structural and mechanical behavior of AA 2024/6063 aluminum alloy couples joined by friction stir welding using different welding parameters, the following conclusions can be made.

- The AA2024 and AA6063 aluminum couples with a thickness of 8 mm were successfully joined by friction welding process without any defects. The welded joints can be divided into several weld zones of SZ, TMAZ, and HAZ the formation of which is considered closely related with plastic flow and frictional heat generation during the welding process.
- The highest tensile strength reaches at S3 sample as 348 MPa which was 74% of the tensile strength of the AA2024 base metal. However, an increasing in tensile strength is present approximately 45% greater than the base tensile strength of AA6063. All tensile failures occurred at HAZ location always at the AA 6063 side. At room temperature material showed some ductility with fracture and revealed local ductile characterization. The fractographic analyses of the tensile tested surfaces revealed that the size distribution of ductile dimples became more circular and wider with higher rotational speed.
- From fatigue analyses of 2024/6063 couple, all samples showed classic fatigue properties of Al alloys. By using lower rotational and higher traverse speed in all welding conditions, the Wohler curves were exhibited maximum fatigue strength for dissimilar Al alloys. The fracture surfaces of the samples exhibit conventional fatigue crack initiation near the surface of the samples. In addition microscopic crack growth and fatigue direction have also been presented and associated with some degree of material ductile.

References

[1] Thomas, W. M., Nicholas, E. D., Friction Stir Welding for the Transportation Industries, *Mater Des*, *18* (1997), 4-6, pp. 269-273
[2] Elangovan, K., Balasubramanian, V., Influences of Pin Profile and Rotational Speed of the Tool on the Formation of Friction Stir Processing Zone in AA2219 Aluminium Alloy, *Mater. Sci. and Eng., A*, *459* (2007), 1-2, pp. 7-18
[3] Kim, Y. G., *et al.*, Three Defect Types in Friction Stir Welding of Aluminum Die Casting Alloy, *Mater. Sci. and Eng., A, 415* (2006), 1-2, pp. 250-254
[4] Cabello, M. A., *et al.,* Comparison of TIG Welded and Friction Stir Welded Al-4.5Mg-0.26Sc Alloy, *J. Mater. Process Technol., 197* (2008), 1-3, pp. 332-343
[5] Yong, P., *at al.*, Comparison of Electrochemical Behaviors between FSW and MIG Joints for 6082 Aluminum Alloy, *Rare Metal Mater. Eng., 46* (2017), 2, pp. 344-348
[6] Cavaliere, P., *et al.*, Effect of Welding Parameters on Mechanical and Micro-structural Properties of AA6056 Joints Produced by Friction Stir Welding, *J. Mater. Process Technol., 180* (2006), 1-3, pp. 263-270
[7] Mishra, R. S., Ma, Z. Y., Friction Stir Welding and Processing, *Mater. Sci. and Eng., R: Rep, 50* (2005), 1-2, pp. 1-78
[8] Rao, M. S., *et al.*, Experimental Study on the Effect of Welding Parameters and Tool Pin Profiles on the IS:65032 Aluminum Alloy FSW Joints, *Mater. Today: Proc, 4* (2017), 2, pp. 1394-1404

[9] Lee, W. B., *et al.,* The Mechanical Properties Related to the Dominant Microstructure in the Weld Zone of Dissimilar Formed Al Alloy Joints by Friction Stir Welding, *J. Mater. Sci., 38* (2003), 20, pp. 4183-4191
[10] Khan, N. Z., *et al.*, Investigations on Tunneling and Kissing Bond Defects in FSW Joints for Dissimilar Aluminum Alloys, *J. Alloys Comp., 648* (2015), Nov., pp. 360-367
[11] Sato, Y. S., *et al.*, Microstructural Evolution of 6063 Aluminum during Friction-Stir Welding, *Metall and Mater. Trans. A, 30* (1999), 9, pp. 2429-2437
[12] Fujii, H., *et al.*, Effect of Tool Shape on Mechanical Properties and Microstructure of Friction Stir Welded Aluminum Alloys, *Mater. Sci. and Eng. A, 419* (2006), 1-2, pp. 25-31
[13] Kim, X. G., *et al.*, Effect of Welding Parameters on Microstructure in the Stir Zone of FSW Joints of Aluminum Die Casting Alloy, *Mater. Let., 60* (2006), 29-30, pp. 3830-3837
[14] Sato, Y. S., *et al.*, Precipitation Sequence in Friction Stir Weld of 6063 Aluminum during Aging, *Metall. and Mater. Trans. A, 30* (2001), 12, pp. 3125-3130
[15] Cavaliere, P., *et al.*, Mechanical and Microstructural Behaviour of 2024-7075 Aluminium Alloy Sheets Joined by Friction Stir Welding, *Int. J. Mach Tools Manuf., 46* (2006), 6, pp. 588-594
[16] Cavaliere, P., Effect of Friction Stir Processing on the Fatigue Properties of a Zr-Modified 2014 Aluminium Alloy, *Mater. Charac., 57* (2006), 2, pp. 100-104
[17] Jata, K. V., Semiatin, S. L., Continuous Dynamic Recrystallization during Friction Stir Welding of High Strength Aluminum Alloys, *Scripta Mater., 43* (2000), 8, pp. 743-749
[18] Okamura, H., *et al.*, Friction Stir Welding of Aluminum Alloy and Application to Structure (in Japanise), *J. Japan Ins. L. Metals, 50* (2000), pp. 166-172
[19] Scialpi, A., *et al.*, Influence of Shoulder Geometry on Microstructure and Mechanical Properties of Friction Stir Welded 6082 Aluminium Alloy, *Mater. Des., 28* (2007), 4, pp. 1124-1129
[20] Jata, K. V., *et al.*, Friction-Stir Welding Effects on Microstructure and Fatigue of Aluminum Alloy 7050-T7451, *Metall Mater. Trans. A, 31* (2000), 9, pp. 2181-2192
[21] Kırık, I., *et al.*, Microstructure and Mechanical Behaviour of Friction Welded AISI 2205/AISI 1040 Steel Joints, *Mater. Testing, 54* (2012), Oct., pp. 683-687
[22] Moreira, P. M. G. P., *et al.*, Fatigue Behaviour of FSW and MIG Weldments for Two Aluminium Alloys, *Theo. Appl. Fracture Mech., 48* (2007), 2, pp. 169-177
[23] Rodriguez, R. I., *et al.*, Low-Cycle Fatigue of Dissimilar Friction Stir Welded Aluminum Alloys, *Mater. Sci. Eng. A, 654* (2016), Jan., pp. 236-248
[24] Kermanidis, A. T., Tzamtzis, A., An Experimental Approach for Estimating the Effect of Heat Affected Zone (HAZ) Microstructural Gradient on Fatigue Crack Growth Rate in Aluminum Alloy FSW, *Mater. Sci. Eng. A, 691* (2017), Apr., pp. 110-120
[25] Nanninga, N., *et al.*, Effect of Specimen Orientation and Extrusion Welds on the Fatigue Life of an AA6063 Alloy, *Int. J. Fatigue, 32* (2010), 2, pp. 238-246
[26] Bystritskii, V., *et al.*, Fatigue Properties of 2024-T3, 7075-T6 Aluminum Alloys Modified Using Plasma-Enhanced Ion Beams, *Theo. Appl. Fracture Mech., 32* (1999), 1, pp. 47-53
[27] Gates, N. R., Fatemi, A., Fatigue Life of 2024-T3 Aluminum under Variable Amplitude Multiaxial Loadings: Experimental Results and Predictions, *Procedia Eng., 101* (2015), Dec., pp. 159-168
[28] Deng, C., *et al.*, Effects of Microstructural Heterogeneity on Very High Cycle Fatigue Properties of 7050-T7451 Aluminum Alloy Friction Stir Butt Welds, *Int. J. Fatigue, 83* (2016), 2, pp. 100-108

Paper submitted: August 25, 2017
Paper revised: November 9, 2017
Paper accepted: November 18, 2017